Carrier Relaxation Times in InAs/AlAs Superlattices: Modulating by Layers, Temperature, and Carrier Concentrations

Enrui Zhang[1,2], Jinshan Yao[3,4], Zhiming Geng[3,4], Yueying Hou[3,4], Jiayu Dai[1,2*], and Hong Lu[3,4*]

[1]*College of Science, National University of Defense Technology, Changsha 410073, China*
[2]*Hunan Key Laboratory of Extreme Matter and Applications, National University of Defense Technology, Changsha 410073, China*
[3]*National Laboratory of Solid State Microstructures, Nanjing University, Nanjing 210093, China*
[4]*Department of Materials Science and Engineering, College of Engineering and Applied Sciences, Nanjing University, Nanjing 210093, China*

(Received 15 December 2024; accepted manuscript online 24 January 2025)

InAs/AlAs superlattice structures have significant potential for application in low-noise avalanche photodetectors. With their performance in practical applications linked to the fundamental physical properties of carrier relaxation time, this study investigated the carrier relaxation times of InAs/AlAs superlattices across various monolayers, temperatures, and carrier concentrations. Our investigation indicated that relaxation times span several tens of picoseconds, confirming that high-quality interfaces do not significantly reduce relaxation times in the way defect states might. Moreover, our study demonstrates that adjustments to the superlattice period can effectively modulate both the bandgap and carrier relaxation times, potentially impacting the performance of avalanche photodiodes by altering the electron–phonon interaction pathways and bandgap width. We established that lower temperatures contribute to an increase in the bandgap and the suppression of high-frequency optical phonon vibrations, thereby lengthening the relaxation times. Additionally, our observations indicate that in InAs/AlAs superlattices, the relaxation time increases as the excitation power increases, owing to the phonon bottleneck effect. These insights into InAs/AlAs superlattice carrier dynamics highlight their applicability in enhancing avalanche photodetectors, and may contribute to the optimized design of superlattices for specific applications.

DOI: 10.1088/0256-307X/42/2/028501 CSTR: 32039.14.0256-307X.42.2.028501

Avalanche photodiodes (APDs) represent a class of semiconductor devices with promising capabilities[1] characterized by their high sensitivities and rapid response rates. These attributes render them indispensable in fields requiring exceptional detection sensitivities, such as fiber-optic communications,[2] Lidar systems,[3,4] medical imaging,[5,6] and quantum communications.[7,8] However, the deployment of APDs at high gains introduces challenges, including precise bias voltage control[9] and reduction of avalanche-induced noise levels.[10,11] According to the local field model,[12] the key to minimizing avalanche noise is to maximize the disparity between the hole ionization rates (β) and electron ionization rates (α), aiming for either significantly large or small ratios of these two rates k. To achieve this goal, researchers have pursued bandgap engineering. In the InAlAs system, the introduction of an InAs/AlAs superlattice alters the band structure by introducing minigaps.[13–15] Electrons within the conduction band can traverse these minigaps through electron–electron scattering, thus maintaining a relatively constant electron ionization rate. However, owing to their special valence-band structure, holes struggle to transition through these minigaps. This leads to the localization of the momentum of the holes and prevents the external electric field from accelerating them, thereby reducing the hole ionization rate. Such effects yielded devices with ultra-low k values of 0.01,[13] indicating a higher signal-to-noise ratio compared with traditional random InAlAs structures.

Carrier dynamics describe the properties of electrons and holes. Thus, to some extent, the carrier relaxation time reflects the ionization rates of electrons and holes in materials.[16,17] For instance, after being excited to the conduction band by photons, electrons are in a non-equilibrium state and move towards a lower-energy state by releasing energy through electron–electron scattering and electron–optical-phonon scattering.[18] A shorter relaxation time from a high- to a low-energy state indicates a rapid loss of electron energy, which reduces the electron ionization rate.[19] Once electrons reach the bottom of the conduction band, the longer they remain there, the more likely they are to be reionized in the depletion layer, thereby increasing the ionization rate.[15] Factors such as the superlattice bandgap, temperature, and carrier density affect the carrier dynamics, as discussed in previous studies for other superlattices, including doped GaAs/AlGaAs[20] and perovskite superlattices.[21] Therefore, exploring the carrier relaxation times of different InAl/AlAs superlattice systems, under various tempera-

*Corresponding author. Email: jydai@nudt.edu.cn; hlu@nju.edu.cn
© 2025 Chinese Physical Society and IOP Publishing Ltd. All rights, including for text and data mining, AI training, and similar technologies, are reserved.

tures and excitation light intensities, is particularly crucial. The pump–probe technique is an effective method for studying this dynamic behavior because of its femtosecond temporal resolution capability and advantages in presenting carrier characteristics. It has been widely used in superlattices to better understand their physical properties and further application.[22–25]

In this study, we first investigated the carrier relaxation times of InAs/AlAs superlattices with different monolayer (ML) configurations at room temperature using ultrafast pump–probe techniques. Then, we analyzed the physical processes reflected by transient reflectivity. Subsequently, using a 4-ML superlattice sample as an example, we compared the carrier relaxation times at various temperatures. Finally, by altering the pump pulse intensity, we examined the changes in carrier relaxation times in InAs/AlAs superlattices at different carrier concentrations.

The carrier relaxation times of InAs/AlAs superlattices were investigated using a femtosecond pump–probe system, as shown in Fig. 1. The system utilized a laser oscillator with a wavelength of 800 nm and a repetition rate of 80 MHz. A portion of the light output from the laser oscillator served as the pump light, which directly acted on the sample. After passing through an optical parametric oscillator (OPO) for wavelength modification, another portion was used as probe light to detect the transient reflectivity of the sample. The pump light had a pulse width of approximately 160 fs with a beam radius of 30.1 μm and a pump power ranging from 5 to 20 mW. The probe light had a pulse width of approximately 200 fs and a radius of 17.5 μm and operated within the wavelength range of 1050–1300 nm. Throughout all tests, the intensity of the probe light was maintained at less than one-tenth of the pump light intensity to minimize its impact on the samples. The pump light was amplitude modulated at 1 MHz using an electro-optic modulator to enhance the signal-to-noise ratio of the pump–probe system. Subsequently, the probe light signal was demodulated using a lock-in amplifier with a time constant of 30 ms. The samples used for the tests were provided by Prof. Lu's group. All the InAs/AlAs superlattices were grown in a Veeco GENxplor MBE system with solid sources of Al, In, and As_2. All the superlattices were grown on semi-insulating InP (001) substrates. After oxide desorption

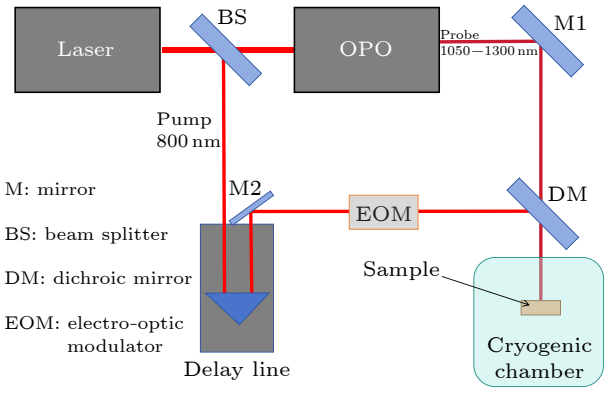

Fig. 1. Schematic of the ultrafast pump-probe system.

from the substrate, a 100-nm-thick $In_{0.52}Al_{0.48}As$ buffer was grown at 490 ℃ to smooth out the InP surface. The substrate temperature was then lowered to the desired temperature to grow the InAs/AlAs superlattices. A series of $InAs_{n\mathrm{ML}}/AlAs_{n\mathrm{ML}}$ ($n = 3$, 4, 5; corresponding to 3 ML, 4 ML, and 5 ML superlattices) superlattices were grown with the same thickness (255 ± 3 nm). The superlattices were finished with n-ML InAs to avoid surface oxidation. Further growth details regarding the superlattices have been reported previously.[26]

This study first investigated the carrier relaxation times of superlattices with different monolayers at room temperature, and the results are presented in Fig. 2. The pump power was 20 mW. For each sample, the relative change in the reflectivity around time zero shifted from positive to negative as the probe wavelength increased. These changes in the reflectivity can be attributed to variations in the transient refractive index, as determined using the Fresnel reflection formula:

$$\Delta R = \frac{\partial R}{\partial n}\Delta n + \frac{\partial R}{\partial k}\Delta k, \tag{1}$$

where n and k are the real and imaginary parts of the refractive index, respectively. Based on the ellipsometry results obtained by Yao *et al.*,[27] by substituting

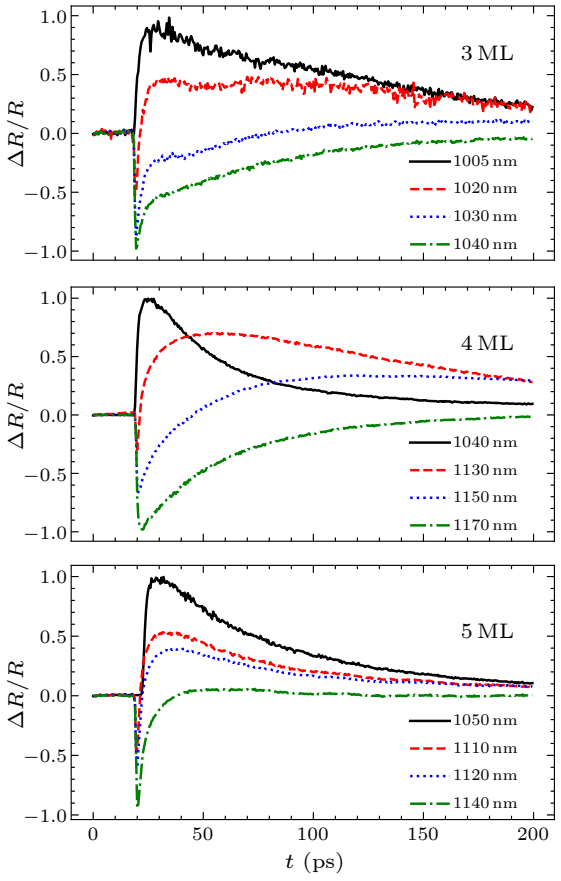

Fig. 2. Transient reflectance of superlattices with different monolayers at room temperature. As the probe wavelength increases, the transient reflectance at $t = 0$ transitions from positive to negative. For probe photon energies around the bandgap, the transient reflectance decreases at first and then increases with time.

the refractive index $n = 3.35$ and $k = 0.01$ for the 3-ML superlattice at 1005 nm, the values for $\frac{\partial R}{\partial n}$ and $\frac{\partial R}{\partial k}$ are approximately equal to 0.114 and 0.75×10^{-3}, respectively. Given that $\frac{\partial R}{\partial n}$ is significantly larger than $\frac{\partial R}{\partial k}$, and that typically Δn and Δk are of the same order of magnitude,[28,29] we can infer that the change in transient reflectivity is caused by the transition from positive to negative in the transient change of the real part of the refractive index as the wavelength increases. The trend of the real part of the refractive-index change implies a decrease in absorption within a specific wavelength range of the sample.[28] By comparing the wavelengths at which the refractive index changes with the photoluminescence (PL) spectrum of the sample,[26] we can conclude that the band-filling (BF) effects lead to a reduction in the light absorption of the sample near the bandgap, which in turn causes the real part of the transient refractive index to change from positive to negative as the wavelength increases.[30] Notably, the wavelengths at which the reflectivity shifted from positive to negative did not exactly match the peak wavelengths of the PL spectrum. This discrepancy can be attributed to the influence of free carriers on the refractive index.[31] In addition, at a pump power of 20 mW, the excited carrier concentration was approximately $8 \times 10^{18}/\text{cm}^3$. A high carrier concentration enhances the many-body effects during carrier interactions, leading to bandgap renormalization (BGR) effects in the sample,[32] which may also cause a discrepancy.

The transient reflectivity at different moments exhibits a trend of decreasing then increasing at a certain probe photon energy. We speculate that this is mainly due to the competition between the BF and BGR effects. Taking the sample with three monolayers (3 ML) and a probe photon energy of 1.22 eV (corresponding to a wavelength of 1020 nm) as an example, the BF effect causes a positive change in the refractive index Δn_{BF} near this photon energy, whereas BGR may enhance absorption at this photon energy, leading to a negative Δn_{BGR}. Typically, owing to the phonon bottleneck effect, the relaxation of the BF effect occurs more slowly than that of the BGR, resulting in reflectivity showing a trend of first decreasing and then increasing.

There were significant differences in the carrier relaxation times of samples with different numbers of monolayers. Figure 3 shows the corresponding experimental results. The probe-light photon energy used in the experiments was greater than the bandgap of the respective samples, primarily to minimize the influence of the BGR effect on the fitting results. Using a single-exponential fit to determine the carrier relaxation times of the different samples, we found that the 3-ML sample exhibited slower relaxation than the other two samples. This could be due to the increased number of atomic units in the superlattice, which enriches and complicates the electron energy states and phonon vibration modes, subsequently accelerating the electron–electron scattering and electron–phonon coupling processes in the material. However, the reasons why the 5-ML sample relaxes slower than the 4-ML sample requires further investigation.

In practical applications, thermal noise in near-infrared photodetectors has garnered widespread attention.[10,11] One effective method for controlling thermal noise is to control the temperature of the photodiode, making studying the carrier relaxation times at different temperatures essential. Figure 4 compares the transient reflectivities of 4-ML superlattice sample at various temperatures for a probe photon energy of 1.15 eV. We observe that the carrier relaxation becomes faster as the temperature increases up to 190 K. This is because high-frequency optical branch phonons cannot be effectively excited at low temperatures, which hinders energy transfer from the electrons to optical phonons. The carrier relaxation process remained almost unchanged when the temperature exceeded 190 K. This indicates that the Debye temperature for InAs/AlAs is approximately 190 K. Furthermore, at 280 K, the transient reflectivity increased directly, indicating that at 280 K, the bandgap is smaller than the photon energy of the probing light. Further observations at 10 K showed that the transient reflectivity first decreased and then increased, indicating that as the temperature decreased, the bandgap of the sample increased and approached the photon energy of the probing light. This phenomenon is primarily associated with the impact of temperature on the lattice structure. As the temperature decreases, the reduction in the lattice constants leads to an increased overlap of electron wavefunctions between atoms, enhancing interatomic bond energy and causing an increase in the bandgap width.

The relaxation time is also related to the pump light power. Figure 5 displays the test results for a 4-ML sample under pump light powers of 5 mW, 10 mW, and 20 mW. The results show that the higher the pump light power, the more significant the change in reflectivity. By examining the maximum and minimum values of $\Delta R/R$ under different excitation powers, the response of the sample to the pump light at 10 mW was notably twice that at 5 mW. However, as the pump energy was increased to 20 mW, the response of the sample no longer doubled that at 10 mW.

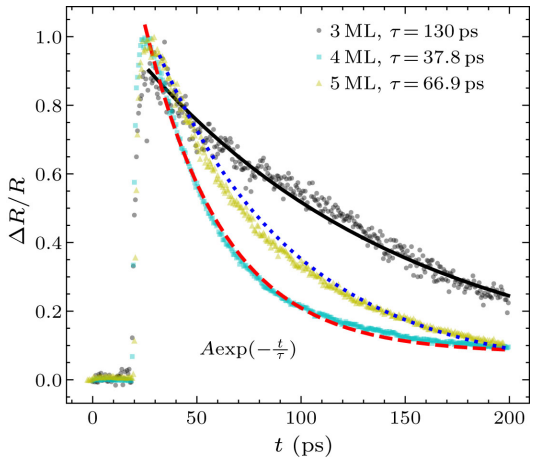

Fig. 3. Comparison of carrier relaxation times in superlattices with different numbers of monolayers. For the 3-ML, 4-ML, and 5-ML superlattices, the probe-light photon energies are 1.23, 1.19, and 1.18 eV, respectively. Because there are more electron–phonon relaxation channels than in the 3-ML superlattice, the 4-ML and 5-ML superlattices exhibited faster carrier relaxation.

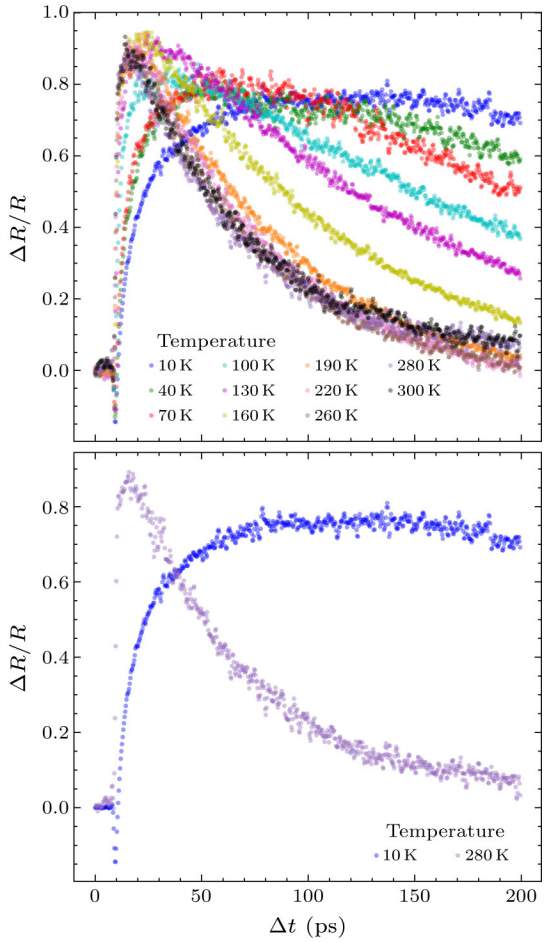

Fig. 4. Comparison of the transient reflectance of the 4-ML superlattice from 10 to 300 K. The bandgap of the superlattice can be inferred to increase as the temperature decreases. Furthermore, below 190 K, high-frequency phonons cannot be effectively excited, resulting in slower carrier relaxation with decreasing temperature.

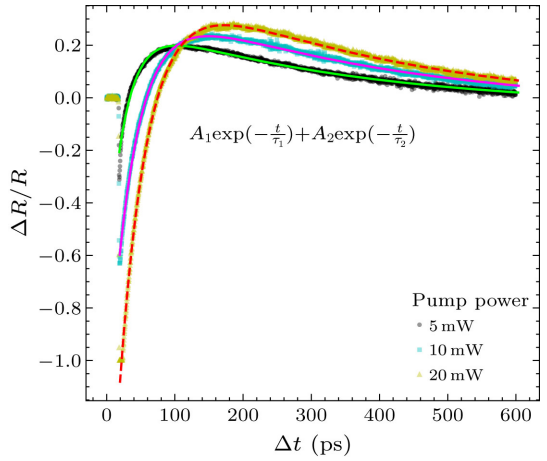

Fig. 5. Transient reflectance of a 4-ML superlattice at room temperature under different pump excitation powers. The probe wavelength was 1130 nm.

This was attributed to the bleaching effect of the ground state at higher pump light intensities, which reduced the absorption of the pump light by the sample. Subsequently, a bi-exponential model was used to fit the relaxation times under different pump light powers. The fitted parameters are listed in Table 1. The results reveal that the relaxation time increased with excitation light power. This is primarily owing to the phonon bottleneck effect, which implies that at higher carrier concentrations, there are not enough optical branch phonons available to participate in the cooling of the carriers, thereby extending their relaxation times.

Table 1. Parameters obtained from fitting the double-exponential model to the transient reflectivities of the 4-ML superlattice under different pump powers.

Pump power	A_1	τ_1 (ps)	A_2	τ_2 (ps)
5 mW	1.4×10^{-3}	336.7	-2.2×10^{-3}	26.1
10 mW	1.9×10^{-3}	363.6	-4.4×10^{-3}	37.9
20 mW	2.4×10^{-3}	357.6	-7.0×10^{-3}	44.0

In conclusion, we explored the relaxation times of samples with different numbers of monolayers at various temperatures and carrier concentrations. Overall, the relaxation times of the InAs/AlAs superlattices were on the order of several tens of picoseconds. This demonstrates that the introduction of high-quality interfaces does not significantly shorten the relaxation time of the material like introducing defect states would. This ensured that the InAs/AlAs superlattices maintained a good photoelectric response when applied. Moreover, the superlattice period can be used to modulate the bandgap and carrier relaxation time. As the structural periodicity increased, the bandgap of the superlattice decreased. Simultaneously, an increase in the number of atoms within the unit cell introduces more phonon vibration modes and electron energy states, thereby increasing the number of pathways for electron–phonon interactions and reducing the relaxation time. The carrier properties of InAs/AlAs superlattices are also influenced by the temperature. At low temperatures, the bandgap increases and the vibration of high-frequency optical branch phonons is suppressed. These combined effects resulted in longer carrier relaxation times at low temperatures. By varying the pump light power, we discovered that at a pump light power of 20 mW, the 4-ML superlattice exhibited reduced absorption of the pump light owing to the ground-state bleaching effect. However, as the excitation light power increased, the phonon bottleneck effect caused the carrier relaxation to slow. Compared with InAs/GaSb and InAs/GaAsSb superlattices, which have been used in mid-infrared photodetectors,[33–38] InAs/AlAs superlattices exhibit a wider bandgap, making them suitable for the high-speed detection of near-infrared light in communication bands. Compared to InGaAs/InAlAs superlattices that have been employed for 1.55 μm detection,[39,40] the growth process of InAs/AlAs is more controllable and offers a wider range of bandgap tuning.[26] In summary, InAs/AlAs superlattices exhibited relatively long carrier relaxation times. This trait, coupled with the tunability of the bandgap and carrier relaxation times through structural period variations and temperature adjustments, allows for a high degree of optimization tailored to specific application demands.

Acknowledgements. This study was supported by the Science and Technology Innovation Program of Hunan Province (Grant No. 2021RC4026).

References

[1] Campbell J C 2015 *J. Lightwave Technol.* **34** 278
[2] Nada M, Yamada Y, and Matsuzaki H 2018 *IEEE Journal of Selected Topics in Quantum Electronics* **24** 1
[3] Kuzmenko K, Vines P, Halimi A, Collins R J, Maccarone A, McCarthy A, Greener Z M, Kirdoda J, Dumas D C, Llin L F *et al.* 2020 *Opt. Express* **28** 1330
[4] Morimoto K, Ardelean A, Wu M L, Ulku A C, Antolovic I M, Bruschini C, and Charbon E 2020 *Optica* **7** 346
[5] Lozovoy K A, Douhan R M, Dirko V V, Deeb H, Khomyakova K I, Kukenov O I, Sokolov A S, Akimenko N Y, and Kokhanenko A P 2023 *Nanomaterials* **13** 3078
[6] Palubiak D, El-Desouki M M, Marinov O, Deen M J, and Fang Q 2011 *IEEE Sensors Journal* **11** 2401
[7] Jiang X, Itzler M, O'Donnell K, Entwistle M, Owens M, Slomkowski K, and Rangwala S 2014 *IEEE journal of selected topics in quantum electronics* **21** 5
[8] Yang M, Xu F, Ren J G, Yin J, Li Y, Cao Y, Shen Q, Yong H L, Zhang L, Liao S K *et al.* 2019 *Opt. Express* **27** 36114
[9] Cova S, Ghioni M, Lacaita A, Samori C, and Zappa F 1996 *Appl. Opt.* **35** 1956
[10] Woodson M E, Ren M, Maddox S J, Chen Y, Bank S R, and Campbell J C 2016 *Appl. Phys. Lett.* **108** 081102
[11] Jones A H, March S D, Bank S R, and Campbell J C 2020 *Nat. Photonics* **14** 559
[12] McIntyre R J 1966 *IEEE Transactions on Electron Devices* p. 164
[13] Zheng J, Yuan Y, Tan Y, Peng Y, Rockwell A K, Bank S R, Ghosh A W, and Campbell J C 2018 *Journal of Lightwave Technology* **36** 3580
[14] Ahmed S Z, Tan Y, Zheng J, Campbell J C, and Ghosh A W 2018 *IEEE Photonics Conference* p. 1
[15] Ahmed S Z, Tan Y, Zheng J, Campbell J C, and Ghosh A W 2022 *Phys. Rev. Appl.* **17** 034044
[16] Goodnick S M and Lugli P 1988 *Phys. Rev. B* **38** 10135
[17] Hohenester U, Supancic P, Kocevar P, Zhou X Q, Kütt W, and Kurz H 1993 *Phys. Rev. B* **47** 13233
[18] Othonos A 1998 *J. Appl. Phys.* **83** 1789
[19] Niaz I A, Miah M A R, Yan L, Yu Y, He Z Y, Zhang Y, Zhang A C, Zhou J, Zhang Y H, and Lo Y H 2019 *J. Lightwave Technol.* **37** 5056
[20] Stehr D, Winnerl S, Helm M, Dekorsy T, Roch T, and Strasser G 2006 *Appl. Phys. Lett.* **88** 151108
[21] Lei Y, Li Y, Lu C, Yan Q, Wu Y, Babbe F, Gong H, Zhang S, Zhou J, Wang R *et al.* 2022 *Nature* **608** 317
[22] Liu B, Li Q, Xu Z, and Ge W 2001 *J. Phys.: Condens. Matter* **13** 3923
[23] Mahler F, Tomm J W, Reimann K, Woerner M, Elsaesser T, Flytzanis C, Hoffmann V, and Weyers M 2018 *Phys. Rev. B* **97** 161303
[24] Jostmeier T, Wecker T, Reuter D, As D J, and Betz M 2015 *Appl. Phys. Lett.* **107** 211101
[25] Sun Z, Wang B R, Xu Z Y, Sun B Q, Ji Y, Ni H Q, and Niu Z C 2006 *Chin. Phys. Lett.* **23** 2566
[26] Yao J, Pan R, Wang W, Li C, Chen B, Lu H, and Chen Y F 2021 *Appl. Phys. Lett.* **118** 252103
[27] Yao L, Wang W, Yao J, Lu K, Lu H, Zheng C, and Chen B 2023 *J. Cryst. Growth* **605** 127071
[28] Kuzmenko A B 2005 *Rev. Sci. Instrum.* **76** 083108
[29] Ashoka A, Tamming R R, Girija A V, Bretscher H, Verma S D, Yang S D, Lu C H, Hodgkiss J M, Ritchie D, Chen C *et al.* 2022 *Nat. Commun.* **13** 1437
[30] Ye Z, Jin Z, Jiang Y, Lu Q, Jia M, Qian D, Huang X, Li Z, Peng Y, and Zhu Y 2024 *Chin. Phys. B* **33** 074210
[31] Sabbah A J and Riffe D M 2002 *Phys. Rev. B* **66** 165217
[32] Das Sarma S, Jalabert R, and Yang S R E 1990 *Phys. Rev. B* **41** 8288
[33] Wang G W, Xu Y Q, Guo J, Tang B, Ren Z W, He Z H, and Niu Z C 2010 *Chin. Phys. Lett.* **27** 077305
[34] Chen Y, Chai X, Xie Z, Deng Z, Zhang N, Zhou Y, Xu Z, Chen J, and Chen B 2020 *J. Lightwave Technol.* **38** 939
[35] Rodriguez J B, Plis E, Bishop G, Sharma Y D, Kim H, Dawson L R, and Krishna S 2007 *Appl. Phys. Lett.* **91** 043514
[36] Mohseni H, Razeghi M, Brown G J, and Park Y S 2001 *Appl. Phys. Lett.* **78** 2107
[37] Zhao Y, Teng Y, Miao J J, Wu Q H, Gao J J, Li X, Hao X J, Zhao Y C, Dong X, Xiong M *et al.* 2020 *Chin. Phys. Lett.* **37** 068501
[38] Zhou Y, Chen J X, Xu Z C, Wang F F, Xu Q Q, Xu J J, Bai Z Z, Jin C, and He L 2014 *Chin. Phys. Lett.* **31** 108503
[39] Lenox C, Nie H, Yuan P, Kinsey G, Homles A, Streetman B, and Campbell J 1999 *IEEE Photonics Technology Letters* **11** 1162
[40] Huang J, Guo T Y, Zhang H Y, Xu J B, Fu X J, Yang H, and Niu J B 2010 *Chin. Phys. Lett.* **27** 118502
[41] Daniel R, Almog R, Ron A, Belkin S, and Diamand Y S 2008 *Biosens. Bioelectron.* **24** 882
[42] Capasso F 1985 *Semiconductors and semimetals* (Elsevier) **22** p. 1